Geologie en Mijnbouw **74:** 65–77, 1995.

Pre-Hercynian magmatism in the Eastern Pyrenees (Cap de Creus and Albera Massifs) and its geodynamical setting

M. Navidad[1] & C. Carreras[2]
[1]*Departamento de Petrología y Geoquímica, Facultad de Geologicas, Universidad Complutense de Madrid, Spain;* [2]*Departamento de Geología, Facultad de Ciencias, Universidad Autónoma de Barcelona, Spain*

Received 15 December 1992; accepted in revised form 8 October 1994

Key words: geochemistry, metabasites, orthogneiss, Palaeozoic

Abstract

In the Eastern Pyrenees Hercynian massifs, basic and acid magmatic associations occur in metasedimentary series of probable Cambrian Late Precambrian age. Basic magmatic rocks occur in the lower part of the metasedimentary series as metagabbros and metabasalts derived from low-K tholeiites and quartz-tholeiites. They are characterised by low niobium and thorium contents (< 5 ppm) and their multi-element and REE patterns are flat. They are interpreted as fractionated E-MORB mantle partial melts. Acid magmatic rocks are: 1) Metarhyolites and dacitic metatuffs intercalated at different levels in the series. They are characterised by low to moderate niobium and thorium contents (7–12 ppm). Their multi-element patterns are analogous to those of crustal melts, and the REE patterns are characteristic of progressively fractionated calcalkaline magmas. These rocks are derived from aluminous calcalkaline crustal magmas. 2) Rhyolitic metaporphyries mainly in the upper part of the series, although thin sills are also present in the lower part. These rocks are highly impoverished in incompatible and REE elements and display low titanium, phosphorus and strontium contents. Their REE patterns are flat with a significant europium anomaly. The rocks represent highly differentiated aluminous calcalkaline crustal magmas. 3) A quartz-monzonitic metaporphyry sill in the lowest part of the series. It represents a meta-aluminous magma with alkaline affinity and, although its incompatible element patterns are analogous to those of the metavolcanics, its REE patterns are more fractionated and exhibit a stronger impoverishment in HREE. The assemblage of acid rocks can be ascribed to a magmatic episode developed by crustal partial melting and likely also to subsequent differentiation. The interbedded acid and basic volcanics in the lower part of the series suggest that both magmatic events overlapped in time, although no genetic connection exists since the acid and basic rocks are of crustal and mantle origin respectively. The magmatism probably took place in a continental back-arc basin.

Geological setting

The Hercynian massifs of Cap de Creus and Albera are located at the eastern end of the Axial Zone of the Pyrenees. The Cap de Creus Massif and the southeastern slopes of the Albera Massif are mainly made up of infra-Caradocian metasedimentary sequences that presumably comprise Lower Palaeozoic and Upper Precambrian. The sequences consist predominantly of rather monotonous metapsammitic and metapelite alternations and contain abundant intercalations of acid and basic igneous rocks (Fig. 1). These sequences have been metamorphosed in a low-P, high-T regional metamorphism of Hercynian age. The metamorphism in this area ranges from very low grade to high grade.

The metasedimentary sequences have been subdivided in different series (Fig. 2). The basal Cadaqués series consists of an at least a kilometre thick alternation of mainly greywackes and minor interbedded pelites. The Mas Patiràs series, restricted to the Albera Massif, forms the upper part of the metasedimentary pile in the area. It forms another kilometre-thick monotonous psammitic-pelitic alternation with abundant light-coloured massive quartzites. Both thick monotonous detrital series are separated by black slates or schists of the Montjoi series, lying on top of the

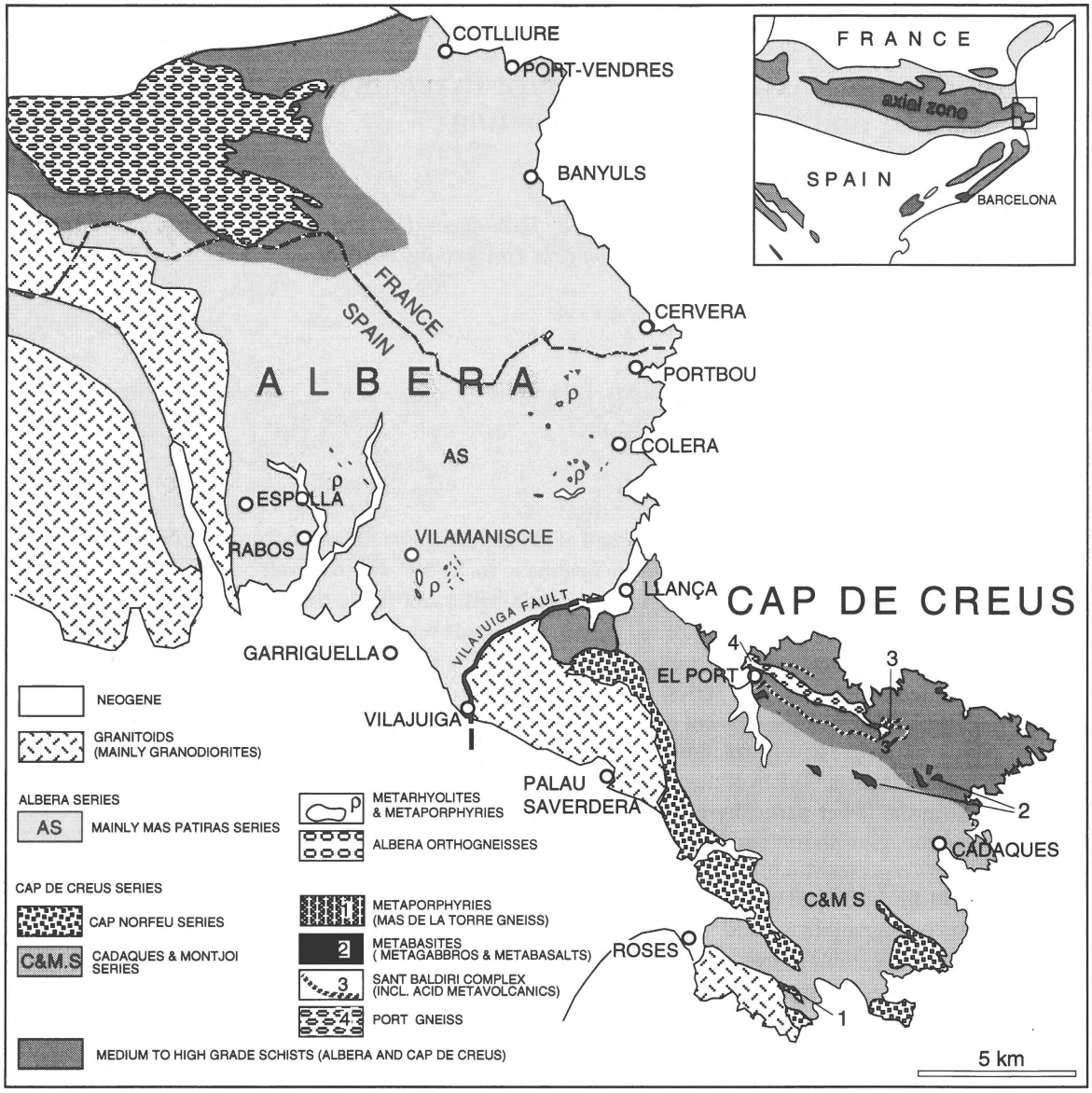

Fig. 1. Simplified geological map of the Cap de Creus and Albera Massifs.

Cadaqués series, and by the overlying clastics and carbonates of the Norfeu series, which form the base of the Mas Patiràs series. The base of the Norfeu series separates the Lower series (Cadaqués and Montjoi) from the Upper series (Norfeu and Mas Patiràs series). Correlation with other areas in the Eastern Pyrenees, on the basis of lithological analogies, suggests that the Cadaqués series could be equivalent to the Balatg schists (Guitard 1970) in the Canigou Massif. All overlying series are tentatively correlated with the Canaveilles and Evol formations outcropping on the northern side of the Canigou gneiss-dome (Laumonier & Guitard 1986; Laumonier 1988). A reliable correlation cannot yet be established due to the absence of palaeontological data.

In the Cap de Creus Massif, pre-Hercynian igneous rocks are preferentially located in the Cadaqués series (Fig. 2). Both acid and basic rocks occur as metamorphosed intrusives (gabbros and porphyries) and extrusives (basalt flows, pyroclastites and ignimbritic flows).

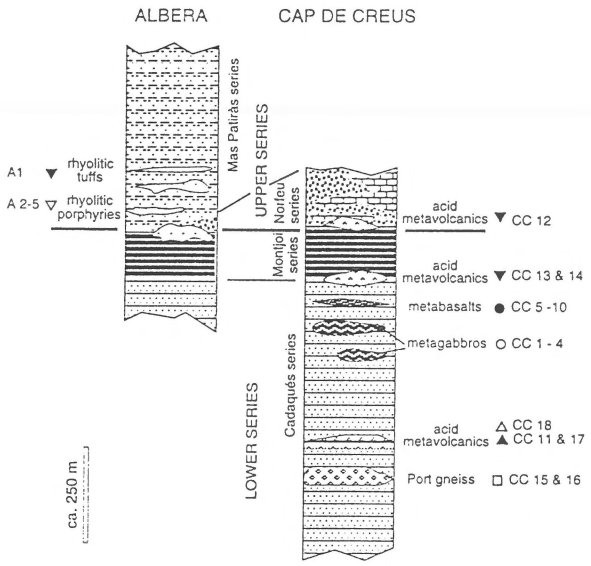

Fig. 2. Schematic stratigraphic sections showing the position of the pre-Hercynian magmatic rocks in metasedimentary series of the Cap de Creus and Albera Massifs. The positions of the analysed samples from these rocks are indicated. For sample symbols see Fig. 3.

Basic rocks occur in the Cadaqués series and have been transformed into amphibolites or greenschists due to Hercynian metamorphism. They form lens-shaped bodies hundreds of metres in length and tens of metres in thickness, and represent a set of sub-volcanic bodies (gabbro-dolerite sills) and basalt lava flows. Due to deformation the gabbro-dolerite bodies are wrapped by the dominant foliation in the enclosing metasediments and exhibit well-foliated, fine-grained margins, while the less deformed cores are texturally heterogeneous with cumulate enclaves and pegmatoid differentiates. Basalt lava flows are approximately 3 m thick and are separated by banded metatuffs and felsic intercalations of hydrothermal origin. Stratigraphically below the metabasites, a unique sill of a metamorphosed subvolcanic intrusion gives rise to the Port gneiss. This sill, up to 200 m thick, displays deformed intrusive features on its margins (Ramirez 1983; Carreras & Ramirez 1984). In this area acid pyroclastic metatuffs are scarce; they occur as lenses with a thickness of decimetres to tens of metres, located preferentially in the upper part of the Cadaqués series, and within the overlying Montjoi and Norfeu series.

In the southern slopes of the Albera Massif, magmatic rocks are predominantly acid and occur mainly in the lowermost part of the Mas Patiràs series as porphyry dykes or irregularly shaped intrusive bodies, but also as lenses of pyroclastic metatuffs. Both intrusive and extrusive rock types are affected by Hercynian deformation and a very low to low-grade metamorphism of the same age. Decametre-thick bodies are foliated on the margins, preserving a porphyritic texture in their cores.

Analytical techniques

Microprobe analyses on plagioclase, amphibole and biotite were performed using an automatic CAMEBAX and a CAMECA SX 50 Electron Microprobe (Laboratoire CAMPARIS Université Pierre et Marie Curie, Paris VI), both equipped with three spectrometers. Operating conditions were: 10 s counting time, 10 nA beam current and 15 kV accelerating voltage. Calibration was made with international standards of the Bureau de Recherches Géologiques et Minières. Amphiboles were classified according to Leake (1978) and the determination of ferric iron from total iron was calculated by charge balance criteria following standard procedures. Analysis of metabasites and acid rocks was performed by inductively coupled plasma and mass spectrometry at the Centre de Recherches Pétrographiques et Géochimiques of Nancy and Laboratoire de Géochimie of Paris VI (cf. Prinzhofer & Allegre 1985; Govindaraju & Mevelle 1987). Major element, trace element and rare-earth element (REE) determinations are shown in Tables 1 and 2. The geochemical treatment has been preferentially carried out on the less mobile elements (Winchester & Floyd 1976, 1977; Humphris & Thompsom 1978; Bienvenu et al. 1990) and the normalised spectrum of incompatible elements (Thompsom et al. 1984) and the REE (Taylor & Mc Lennan 1985).

Petrography and geochemical features

Metabasites

Gabbro-dolerite sills and basalt lava flows were metamorphosed during the Hercynian orogeny under upper-greenschist and lower-amphibolite facies conditions. This produced significant mineralogical modifications, although the original textures were preserved in low-strained domains. Metagabbros display diablastic or lepido-nematoblastic textures. Their mineral assemblages are composed by albitized plagioclase with An_{20-13} and zoned amphibole with a ferrotscher-

Table 1. Chemical composition of Cap de Creus pre-Hercynian metabasites (P.Gbr = pegmatoid metagabbro, Gbr = metagabbro, Bas = metabasalt. Schematic stratigraphic location of samples is shown in Fig. 2). Major element, trace element and REE analyses were performed by inductively coupled plasma spectroscopy (ICP) at the Analyses Service of the Centre de Recherches Pétrographiques et Géochimiques (CRPG de Nancy). Analyses CC4, CC6 and CC9 were performed by mass spectrometry at the Geochemical Laboratory of Paris VI (Analyst: N. Vassard). Fe_2O_3 = total iron as Fe_2O_3.

Rock	P.Gbr	P.Gbr	Gbr	Gbr	Bas	Bas	Bas	Bas	Bas	Bas
Sample no.	CC1	CC2	CC3	CC4	CC5	CC6	CC7	CC8	CC9	CC10
SiO_2	57.75	56.24	51.49	51.58	55.80	56.85	53.32	54.88	52.37	52.60
TiO_2	0.54	1.67	1.36	0.91	1.53	1.55	1.37	1.65	1.26	1.66
Al_2O_3	14.83	13.88	13.89	14.02	14.51	15.06	14.05	14.85	13.96	14.67
Fe_2O_3	6.41	11.53	12.64	1.56	10.91	10.89	11.71	1.84	11.48	12.03
FeO				6.88				8.40		
MnO	0.11	0.17	0.17	0.16	0.24	0.22	0.25	0.22	0.22	0.22
MgO	5.62	3.37	6.39	7.93	4.79	4.66	6.07	5.07	6.83	5.39
CaO	8.73	7.20	8.08	11.63	6.99	7.15	7.49	6.74	8.73	6.41
Na_2O	4.76	4.41	4.19	2.71	3.02	3.19	3.58	4.33	4.10	4.19
K_2O	0.20	0.22	0.32	0.30	0.88	0.71	0.22	0.41	0.14	0.46
P_2O_5	0.17	0.30	0.22	0.07	0.22	0.00	0.22	0.16	0.22	0.26
H_2O	0.67	0.84	1.07	1.36	0.87	0.89	1.46	1.21	0.50	1.91
Total %	99.79	99.83	99.82	99.11	99.76	101.17	99.74	99.76	99.81	99.8
Ba ppm	127	45	67	102	446		122	58	122	60
Be	1	1.7	1.29		1.5		1.79		1.2	1.7
Co	5	25	37	33	35		39	38	27	49
Cr	159	14	151		108		551		181	326
Cu	9	17	49	17	37		42	31	45	56
Ga	29	15	17		31		21		12	21
Nb	7	3	5	5	6		4	5	4	10
Ni	36	14	38	35	31		60	31	37	46
Rb	9	7	11	8	24		6		7	18
Sc	42	43.4	52.7		45.4		50.7		54.4	50.9
Sr	187	169	371	221	327		364	395	340	346
Th	4	4	3		5		3		4	5
V	114	328	291	231	309		296	348	286	370
Y	47	43	30	21	35		33	31	27	36
Zn	51	74	82	57	136		131	92	144	94
Zr	233	159	93	117	117		116	165	76	118
La	11.26	10.67	7.68		11.14		11.19		6.98	11.35
Ce	34.50	34.66	26.28		28.96		47.31		25.50	35.20
Nd	20.58	18.53	11.68		15.96		14.56		10.23	15.71
Sm	6.63	5.97	3.86		5.00		5.07		3.58	5.15
Eu	1.22	1.86	1.21		1.31		1.56		1.15	1.63
Gd	6.95	6.51	4.38		5.24		5.83		4.19	5.44
Dy	8.02	7.73	4.95		5.98		5.75		4.58	5.92
Er	4.89	4.46	2.91		3.69		3.45		2.62	3.45
Yb	4.88	4.55	2.85		3.53		3.34		2.57	3.42
Lu	0.88	0.58	0.38		0.65		0.47		0.32	0.49

Table 2. Chemical composition of pre-Hercynian acid rocks from the Cap de Creus and Albera Massifs. L.Tuff = metatuffs of the Lower series, U.Tuff = metatuffs of the Upper series, P.Gn = quartz-monzonitic metaporphyry (Port gneiss), LP.Rhy = rhyolitic metaporphyries of the Lower series, UP.Rhy = rhyolitic metaporphyries of the Upper series. Schematic stratigraphic location of samples is shown in Fig 2. Major element, trace element and REE analyses were performed as in Table 1. Analyses CC14, A4 and A5 were performed by mass spectrometry at the Geochemical Laboratory of Paris VI (Analist: N.Vassard). Fe_2O_3 = total iron as Fe_2O_3.

Rock	L.Tuff	U.Tuff	L.Tuff	L.Tuff	P.Gn	P.Gn	L.Tuff	LP.Rhy	U.Tuff	UP.Rhy	UP.Rhy	UP.Rhy	UP.Rhy.
Sample no.	CC11	CC12	CC13	CC14	CC15	CC16	CC17	CC18	A1	A2	A3	A4	A5
SiO_2	69.52	72.65	64.29	69.74	65.23	64.12	65.75	76.62	69.54	75.52	76.32	75.65	73.45
TiO_2	0.89	0.81	0.98	0.68	0.37	0.34	0.68	0.03	0.54	0.14	0.10	0.11	0.22
Al_2O_3	14.76	11.39	14.38	15.66	17.06	17.43	15.11	13.46	15.31	13.91	13.42	13.41	14.05
Fe_2O_3	2.00	3.24	6.69	2.78	0.44	2.84	4.62	0.78	3.84	1.62	1.22	0.76	1.01
FeO					2.16							0.49	0.7
MnO	0.02	0.05	0.06	0.02	0.05	0.04	0.13	0.00	0.05	Tr	Tr	0.04	0.01
MgO	1.54	1.46	2.77	0.69	1.4	1.41	2.04	0.03	1.04	0.59	0.25	0.26	0.44
CaO	2.17	4.08	1.45	0.59	3.28	3.33	1.29	0.53	0.38	0.20	0.10	0.10	0.14
Na_2O	2.87	2.27	3.2	3.78	4.92	5.16	7.83	6.52	2.95	2.36	4.47	3.17	3.21
K_2O	3.12	2.52	3.2	4.22	3.38	3.55	0.10	1.13	3.22	3.40	2.62	4.61	4.23
P_2O_5	0.25	0.22	0.3	0.00	1.12	0.17	0.25	0.03	0.22	0.14	0.14	0.07	0.13
H_2O	2.47	1.05	2.7	2.01	0.8	1.3	1.05	0.69	2.88	1.96	1.20	1.35	1.68
Total %	99.61	99.74	100.02	100.17	99.21	99.69	98.85	99.82	99.97	99.84	99.84	100.02	99.27
Ba ppm	1536	641	1663		768	688	61	520	567	363	336	232	774
Be	22	1.2	1.6		4	4.9	1.2	2.09	2.29	2.2	2.5		
Co	5	5	5		5	5	5	104	5	3	5	21	7
Cr	125	94	71		207	9	85	32	20	11	5	21	
Cu	28	21	22		15	14	9	18	11	9	8	10	8
Ga	16	4	23		22	28	35	26		27	16		
Nb	11	10	12		9	10	12	20	14	10	7		8
Ni	6	31	32		23	23	36	4	20	7	5	10	10
Rb	87	52	76		154	149	4	29.5	111	143	82	204	170
Sc	17.7	11.8	18.7		6.4	6.4	12.8		10.3	5.8	5.3		
Sr	185	169	220		513	470	96	90	62	63	113	41	63
Th	5	7	11		11	13	8	7	11	8	5		
V	96	81	111		37	35	84	2	34	14	7	10	11
Y	14	33	42		8	9	23	44	36	26	25	39	31
Zn	38	50	131		44	44	31	7	65	108	5	24	50
Zr	199	246	255		122	119	177	118	227	61	58	98	135
La	32.08	27.46	30.04		25.76	23.93	56.57	9.99	33.50	10.50	9.01		
Ce	64.10	60.73	64.83		51.41	45.94	101.10	22.58	67.46	27.20	23.47		
Nd	26.8	29.17	34.66		17.87	18.55	49.32	12.75	34.42	10.52	9.21		
Sm	5.81	6.91	8.50		3.33	3.68	9.16	4.34	7.79	3.53	3.11		
Eu	1.17	1.24	1.28		0.86	0.86	1.42	0.69	1.16	0.32	0.24		
Gd	4.29	6.06	7.72		2.59	2.68	6.89	4.59	6.93	3.48	3.05		
Dy	3.24	5.98	7.96		1.48	1.69	4.56	6.23	6.46	4.40	4.42		
Er	1.79	3.47	4.58		0.79	1.06	2.45	4.22	3.52	2.53	2.45		
Yb	2.05	3.23	4.35		0.80	0.89	2.34	4.94	3.22	2.90	2.93		
Lu	0.29	0.59	0.77		0.09	0.19	0.48	0.78	0.57	0.34	0.34		

makitic hornblende core and an actinolitic margin transformed in some instances into clinozoisite. Accessories are metastable skeletal ilmenite and allanite transformed to titanite and leucoxene pseudomorphs. Amphiboles with intermediate composition between Mg-hornblende and actinolite, clinozoisite and chlorite are the most common retrometamorphic minerals.

The lava flows are plagioclase basalts with a relict igneous flow texture. A microcrystalline matrix consists of an aggregate of tschermakitic hornblende transformed into Mg-hornblende and actinolitic hornblende, microlithic plagioclase (An_{27-25}) and biotite. Quartz, albite, clinozoisite, epidote and carbonates are the most common retromorphic minerals. Banded ashes are composed by light felsic layers formed by quartz, plagioclase (An_{17-13}) and cummingtonite forming bow-tie aggregates and dark layers consisting of plagioclase, quartz, Mg-hornblende, actinolite, biotite and accessory minerals (ilmenite, magnetite, tourmaline, zircon and apatite).

Analyses of ten metabasite samples from the Cadaqués series are shown in Table 1. All analysed rocks have a similar composition, with slight variations within the gabbros due to the abundance of pegmatoid differentiates (analyses CC1 and CC2). These rocks are not spilitized and are characterised by low potassium, magnesium and nickel contents ($K_2O < 0.5\%$, MgO = 5–7%, Ni < 50 ppm) and variable chrome content (Cr = 100–500 ppm). The niobium and thorium trace elements are remarkably low (< 5 ppm). Nearly all rock samples are quartz and hypersthene normative (Q = 4–10%), except two samples being olivine normative (CC9: 3% and CC3: 6%).

A plot of SiO_2 and Zr/TiO_2 in a Winchester & Floyd (1977) diagram (Fig. 3a) reveals the subalkaline character of this series, made by basalt-andesite and andesite members with low potassium content (Fig. 3b). In an AFM diagram (Fig. 4a) these rocks fall in the middle of the tholeiitic-calcalkaline boundary. However, the data in a FeO_T-Al_2O_3-MgO diagram (Fig. 4b) define a tholeiitic trend with similar relations to those found by Miyashiro (1974).

The incompatible trace elements of the metabasite contents, normalised according to Thompsom et al. (1984) in Fig. 5, show patterns with a flat slope characterised by high thorium enrichment with respect to depleted rubidium and potassium. A marked negative anomaly in niobium and a slight enrichment of the transition elements and depletion of low-incompatibility elements are also manifest. These patterns are slightly different in the pegmatoid metagabbros that show negative anomalies in strontium, phosphorus and titanium related with plagioclase, apatite and titanium mineral fractionation.

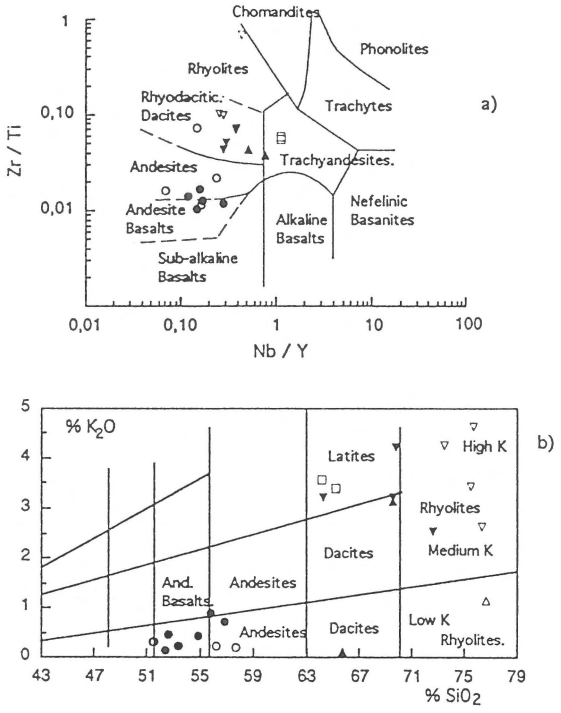

Fig. 3. Distribution and classification of the pre-Hercynian magmatic rocks in diagrams: (a) Zr/TiO_2 against Nb/Y (after Winchester & Floyd 1977). Note that the acid metatuffs from the Lower series are shifted towards the alkaline area. (b) $\%K_2O$ against $\%SiO_2$. The basic rocks are distributed in the low potassium area, while the acid rocks have medium to high potassium content. The rock boundaries are those of Pecerrillo & Taylor (1976). Symbols: •: metabasalt lava flows; ○: metagabbro sills; □: quartz-monzonitic metaporphyries (Port gneiss); ▲: lower pyroclastic metatuffs; ▼: upper pyroclastic metatuffs; △: lower rhyolite metaporphyry; ▽: upper rhyolitic metaporphyries.

The chondrite-normalised REE patterns (Taylor & Mc Lennan 1985) in Fig. 6 show a relatively flat profile with a low fractionation ($(La/Yb)_N$ = 1.56–2.26) and only a significant europium anomaly in one pegmatoid metagabbro (Eu/Eu^* = 0.55). However, there is a cerium anomaly ((Ce/Ce^*) = 0.93–1.29) that could be related to crustal contamination caused by pelitic sediments. The assemblage profiles are parallel, showing a fractionation in the basic rocks.

The Port orthogneiss

The Port orthogneiss is a highly homogeneous, massive and rather leucocratic sill. It displays a recognis-

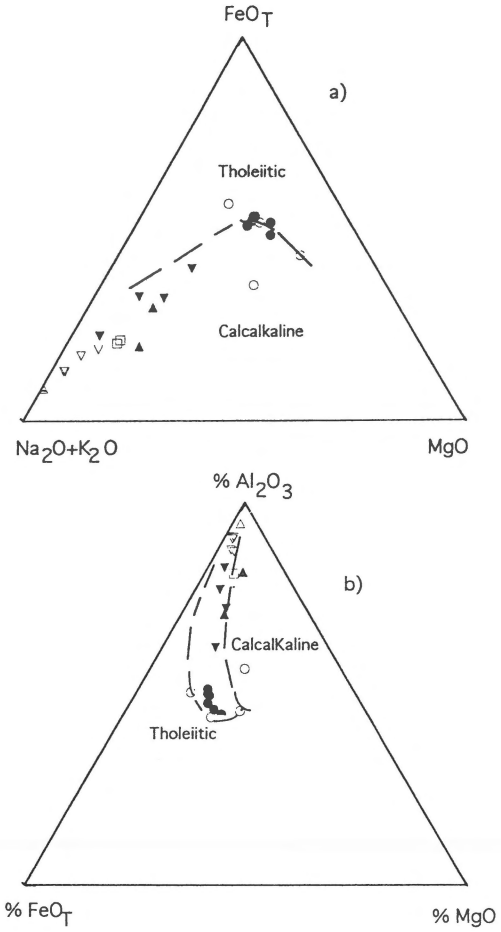

Fig. 4. Distribution of the pre-Hercynian magmatic rocks. Symbols as in Fig 3. (a) AFM classification diagram. The basic rocks plot in the middle of the tholeiitic-calcalkaline boundary line after Kuno (1959), while the acid rocks show a calcalkaline trend. (b) %FeO$_T$-Al$_2$O$_3$-MgO classification diagram. Calcalkaline and tholeiitic trends after Besson & Fonteilles (1974).

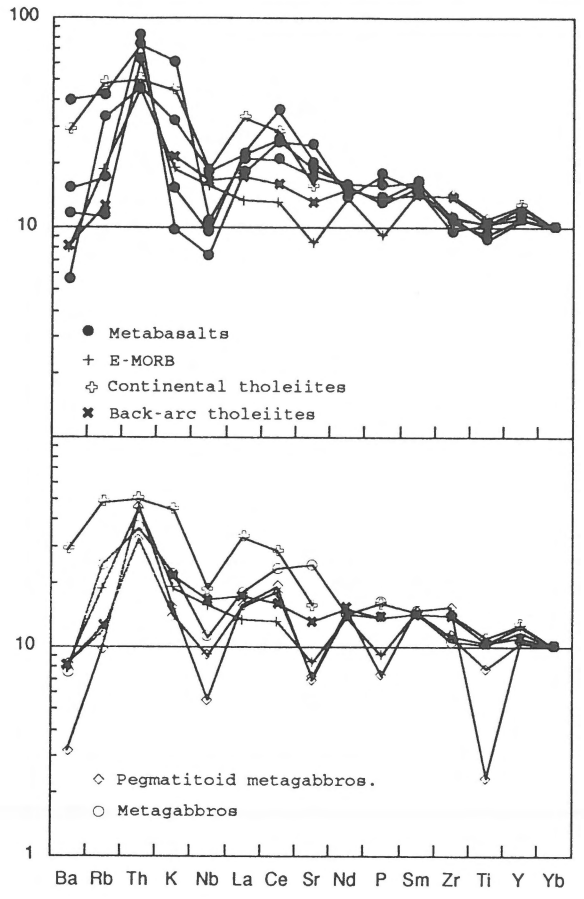

Fig. 5. Multi-element spidergrams for the basic rocks (metabasalts and metagabbros with pegmatoid differentiates) of the Cap de Creus Massif. Chondrite and Rb, K and P normalisation factors after Thompsom et al. (1984). The patterns of the basic rocks are compared with continental tholeiites (Holm 1985), back-arc tholeiites (East Scotia Sea basalts, Saunders & Tarney 1979) and E-MORB (Humphris et al. 1985).

able relict porphyritic texture with sporadic feldspar phenocrysts. The rock has a blastoporphyritic texture with tectonically induced foliation. The gneiss is composed of perthitic microcline, quartz, plagioclase (An_{17}) and biotite. The accessory minerals are zircon, apatite, allanite and abundant titanite. Metablasts composed of microcline containing amphibole, chlorite and albite inclusions and others consisting of polycrystalline albite are also frequent.

Table 2 includes chemical analyses of two samples of the orthogneiss (CC15, CC16). The rocks are meta-aluminous with alkaline affinity ($Na_2O + K_2O > 8\%$) and sodium-potassium character ($Na_2O/K_2O = 1.5$); they contain normative diopside and hypersthene. They plot in the alkaline area according to the Winchester & Floyd (1977) relations (Fig. 3a) and are quartz-monzonitic in composition with regard to the classification of Debon & Le Fort (1983).

Trace elements are characterised by their low niobium, yttrium (< 10 ppm) and zirconium contents (Zr = 119–122 ppm). The incompatible trace element patterns (normalised according to Thompsom et al. 1984; Fig. 7c) show a high enrichment of the high-incompatible elements, followed by a moderate descent of transition elements and a marked depletion of low-incompatible elements. The Port orthogneiss samples are also characterised by their high thorium content; the negative anomalies of niobium and

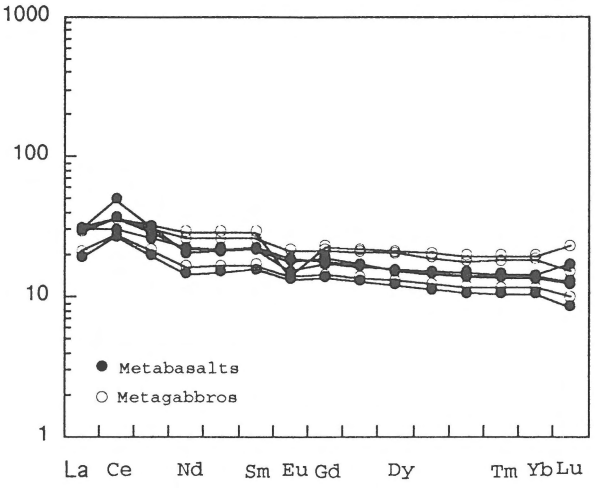

Fig. 6. Chondrite-normalised REE profiles for the Cap de Creus basic rocks. Normalisation factors after Taylor & MacLennan (1985). Note that the profiles are slightly flat with a fractionation between them.

titanium are similar to those found in the metabasic rocks.

The REE content in the orthogneisses is low ($\sum$REE = 98–104). The rocks have highly fractionated patterns ($(La/Yb)_N$ = 18–22) with a light rare-earth (LREE) enrichment (La_N = 77–83) and heavy rare-earth (HREE) depletion (Yb_N = 4), and a nearly imperceptible europium anomaly (Eu/Eu^* = 0.84–0.89, Fig. 8a). Their pattern is consistent with highly differentiated rocks formed by a low degree of partial melting, with garnet as a residual phase.

Acid rocks in the Lower and Upper series

In the Cap de Creus and Albera Massifs there are different types of acid rocks (Fig. 2). In the Lower series (Cadaqués and Montjoi series) feldspathic metatuffs and rhyolitic porphyries are scarce. They form either part of an intercalation in the black schists and marbles of the San Baldiri Complex (Fig. 1), or are located close to or in the Montjoi series (Mas de la Torre gneisses). They form lenses with a thickness of decimetres to tens of metres of strongly foliated rocks with relict albitized K-feldspar and/or albite phenocrysts, enclosed in a microcrystalline matrix formed by abundant quartz, albite, chlorite, sericite and ilmenite.

In the Upper series (Norfeu series in Cap de Creus and Mas Patiràs series in the Albera Massif) abundant metatuffs and sills of rhyolitic porphyries are includ-

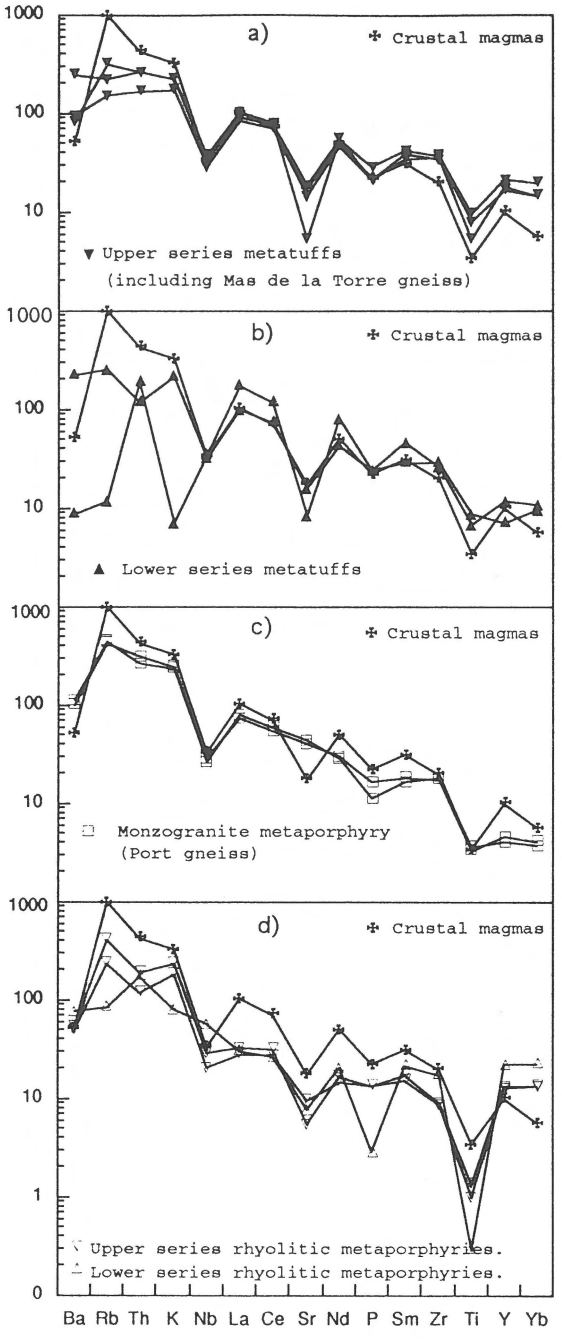

Fig. 7. Multi-element spidergrams for the pre-Hercynian acid magmatic association of the Cap de Creus and Albera Massifs. Chondrite and Rb, K and P normalisation factors after Thompsom et al. (1984). All acid rock patterns are compared with S-type magmas (cordierite rhyodacite of San Vincenzo, Italy; Thompsom et al. 1984).

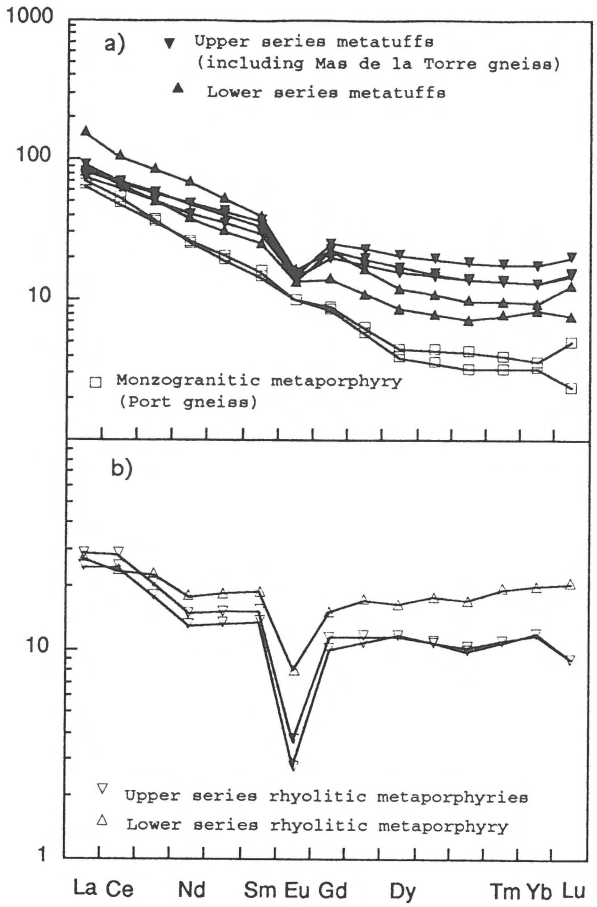

Fig. 8. Chondrite-normalized REE profiles for the pre-Hercynian acid rocks of the Cap de Creus and Albera Massifs. Normalisation factors after Taylor & MacLennan (1985). a) A progressive fractionation is shown for the quartz-monzonitic porphyry (Port gneiss) and the tuffs of the Upper and Lower series. b) The upper and lower rhyolitic metaporphyries patterns are similar.

ed in the low-grade or very low-grade metasediments. The metatuffs, with a thickness of approximately five metres and of rhyodacitic and rhyolitic composition, occasionally preserve relict ignimbrite flow textures and proterogenic crystals of embedded idiomorphic quartz, albitized K-feldspar and plagioclase. In some instances polycrystalline carbonate aggregates of post-magmatic origin appear. Apatite, zircon, leucoxene and pyrite are the most abundant accessories. In the ignimbritic metatuffs, actinolitic amphibole, biotite, albite and ilmenite-leucoxene pseudomorphs after ilmenite are present.

The rhyolitic metaporphyries, all located in the lower part of the Mas Patiràs series in the Albera Massif, are the most abundant manifestations of the acid magmatism and appear as intrusive bodies or interlayered sheets. The rocks are composed of quartz, albitized K-feldspar and albite phenocrysts enclosed in a quartz-feldspathic matrix with residual micropegmatitic and graphic textures.

The chemical compositions are given in Table 2. In the Lower series of the Cap de Creus Massif, samples CC11 and CC17 correspond to metatuffs in the San Baldiri complex and CC18 corresponds to a rhyolitic metaporphyry in the same complex (Figs 1, 2). Metatuff samples CC12, CC13 and CC14 are located in or just above the upper part of the Lower series in the Cap de Creus Massif, while A1 corresponds to a metatuff from the Albera Massif located near the base of the Upper series. Samples A2–5 are rhyolitic metaporphyries emplaced in the Mas Patiràs series of the same massif. The metatuffs in the Lower and Upper series have similar compositions; all plot in the rhyodacite area according to the Winchester & Floyd (1977) classification (Fig. 3a) and have an aluminous character (normative corundum = 4%). However, the potassium content is greater in metatuffs from the upper part of the metasedimentary pile (Fig. 3b). The discriminate trace elements are also similar in all acid metatuffs and slightly higher than in the metabasites (Nb and Th > 10 ppm).

The incompatible trace elements show an analogous behaviour in nearly all acid metatuffs. The patterns (Figs 7a, b) are characterised by a slight negative slope with enrichment of high-incompatible and transition elements and moderate depletion of low-incompatible elements, except one tuff located in the San Baldiri complex of the Cadaqués series (Fig. 7b) that also shows depletion in Ba, Rb and K. All these rocks also exhibit remarkably negative anomalies in niobium, strontium, phosphorus and titanium and show a pattern analogous to the composition of the crustal magmas.

The REE contents of the Lower series metatuffs are slightly higher ($\sum$REE = 142–234) than those of the Upper series metatuffs ($\sum$REE = 144–165). The patterns of these lower metavolcanics are similar to those observed in the Port orthogneiss: highly fractionated ($(La/Yb)_N$ = 10–16), LREE enrichment (La_N = 90–170), HREE depletion (Yb_N = 8–10), and no significant positive europium anomaly (Eu/Eu* = 0.55–0.72, Fig. 8a). However, the metatuffs of the Upper series display less fractionated patterns ($(La/Yb)_N$ = 5–7) with a lower LREE content ($\sum$LREE = 124–143) and a more marked positive anomaly of europium (Eu/Eu* = 0.48–0.59). Patterns of these rocks in the Upper and Lower series are similar and show a

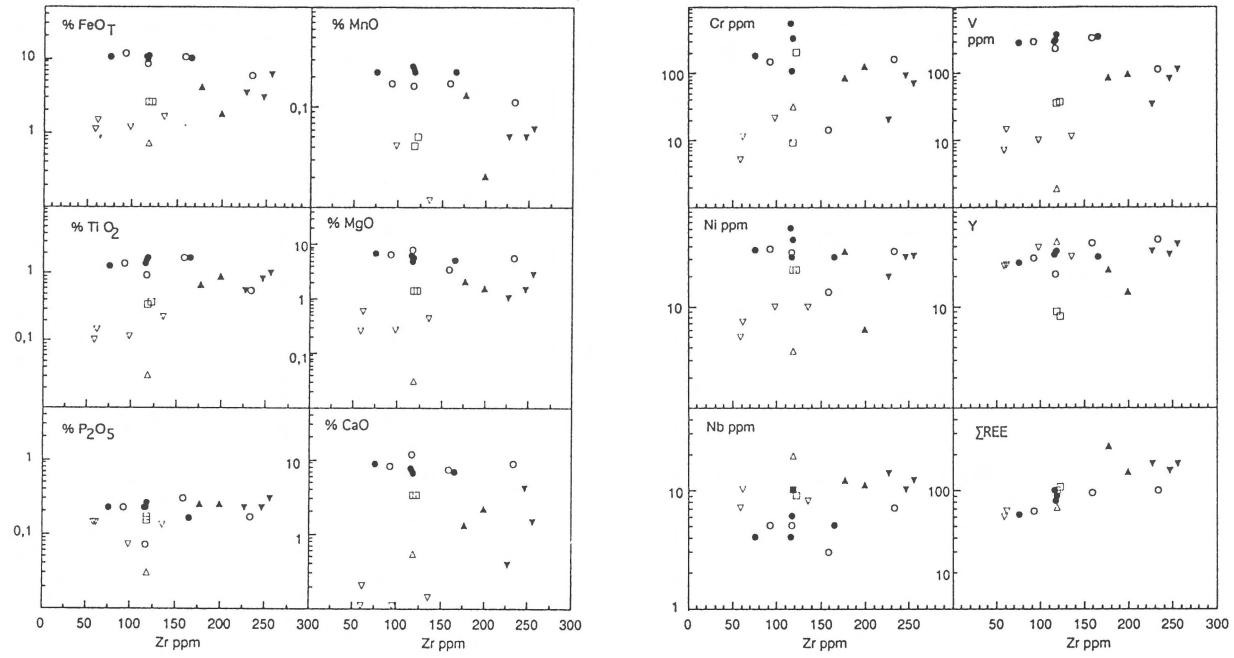

Fig. 9. Binary logarithmic correlation of Zr versus major elements, trace elements and ∑REE of magmatic rocks of the Cap de Creus and Albera Massifs. Symbols as in Fig 3. A correlation appears for the basic rocks, but not between both associations.

progressive fractionation between them and also with the Port orthogneiss.

The five analysed samples of rhyolitic porphyries (Table 2, CC18 and A2–5) show high silica and alkali contents (SiO_2 = 73–77%, alkalis = 5–8%). They are classified as rhyolite members of a calcalkaline series with a variable potassium content (Figs 3a, b). On the other hand, they also correspond to the most impoverished members of this acid magmatic series because they are characterised by a very low phosphorus, titanium and zirconium content (P > 0.14%, Ti < 0.2% and Zr = 58–135 ppm). Their incompatible trace element patterns show a moderate negative slope with slight negative anomalies in strontium, titanium and variable anomalies in niobium (Fig. 7d). The REE contents are also very low (∑REE = 58–77) and the patterns (Fig. 8b) are flat ($(La/Yb)_N$ = 1.37–2.45), with the exception of a lanthanide and cerium enrichment probably due to a concentration of specific mineral phases (i.e., monazite, allanite) in the melt. A marked negative anomaly in europium (Eu/Eu* = 0.24–0.47) reflecting plagioclase fractionation is another characteristic property.

Discussion and interpretation

Investigations of the pre-Caradocian igneous rocks of the Cap de Creus and Albera area clearly confirm the presence of two magmatic associations with different chemical compositions. The first is formed by a plutonic-volcanic association made up of tholeiites and quartz-tholeiites with low potassium content. The second is an aluminous calcalkaline association including tuffs, pyroclastic flows, rhyolitic porphyries and metaaluminous quartz-monzonitic porphyries (orthogneiss) with a more alkaline affinity. Geochemical features suggest a different origin for the two associations.

All the analysed samples have been plotted in AFM and FeO_T-Al_2O_3-MgO diagrams (Figs 4a, b); a calcalkaline trend is evident for the acid rocks (acid metatuffs, rhyolitic porphyries and orthogneiss), but the basic rocks plot in the middle of the tholeiitic-calcalkaline boundary. However, a compositional gap is clearly present between both magmatic associations.

In addition, plots of all samples in the binary correlation diagram between zirconium and the other major and trace elements (Fig. 9) enable to define differ-

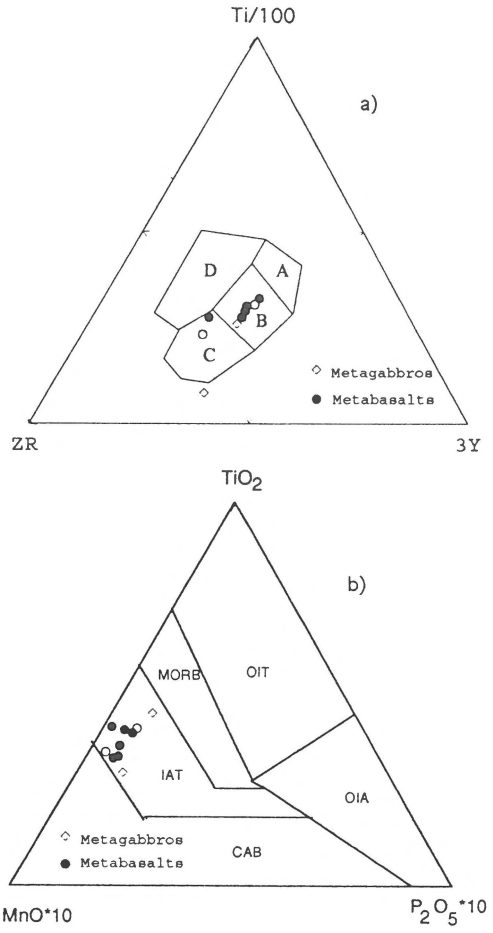

Fig. 10. Geochemical setting of the pre-Hercynian basic rocks of the Cap de Creus Massif. (a) Zr-Ti/100-3Y diagram after Pearce & Cann (1973). Rocks are distributed among the MORB area (B) and calcalkaline area (C) (D = intra-plate area; A = low-potassium tholeiites). (b) MnO-TiO_2-P_2O_5 diagram after Mullen (1983). Rocks plot in the island-arc tholeiites area (IAT); (OIT = ocean island tholeiites; OIA = ocean island alkaline basalts; CAB = calcalkaline basalts).

ent trends for acid rocks and basic rocks with regard to some elements (FeO_T, TiO_2, MnO, CaO, Ni, V, Nb). This suggests that the two associations are non-cogenetic and, furthermore, that they followed different fractionation processes.

The interpretation of incompatible trace elements and REE patterns and the specific relations between the less mobile elements suggests that these magmatic assemblages are related to a continental back-arc basin or a marginal continental basin. The basic rocks, metagabbros and metabasalts (quartz tholeiitic low-potassium type) show very low niobium contents (< 5 ppm), typical of magmas from subductive settings; furthermore, they have high thorium contents in agreement with a continental origin. Their Zr-Ti/100-3Y and MnO*10-TiO_2-P_2O_5*10 ratios (Figs 10a, b) point to analogies with mid-ocean-ridge basalts (MORB) and with arc tholeiites from subductive domains. Data similar to those found in the analysed samples, i.e., intermediate between MORB and arc tholeiites, are frequent in back-arc domains (Knoper & Condie 1988; Cabanis 1986), although they have also been described for continental tholeiites (Dupuy & Dostal 1984). However, the latter are more enriched in the high-incompatible elements and in the LREE. On the other hand, incompatible trace element patterns of metabasites (Fig. 5) are characterised by a rather flat slope with a variable negative anomaly in niobium and titanium and a positive one in strontium; the relatively low content of high-incompatibility elements also defines a positive slope (Rb-Ba-Th), in better accordance with continental back-arc tholeiites (Holm 1985) than with continental tholeiites and enriched mid-ocean-ridge basalts (E-MORB).

Titanium and niobium anomalies are not only present in the basic intrusives of the Early Palaeozoic, but have also been reported in Archaean bimodal suites (Taylor & Mc Lennan 1985). Saunders et al. (1980) suggest that melting of MORB in a hydrous environment (subductive zone) would generate quartz-saturated melts and a residue consisting of zirconium and titanium-rich mineral phases, with a later impoverishment in niobium, titanium and zirconium in the melts. In more differentiated types these anomalies are distinctive and accompanied by lower concentrations of strontium and lead, due to the fractionation of plagioclase and specific mineral phases such as apatite. Similar models by Saunders & Tarney (1979) have been evoked to explain collisional environments in back-arc type settings (i.e., Brouxel et al. 1989; Stolz et al. 1990).

The REE patterns of the metabasite rocks (Fig. 6) are slightly flat and the HREE contents ($\sum$HREE = 14–25) are within the range of E-MORB ($\sum$HREE = 10–17, Humphris et al. 1985) and also of tholeiites originating in evolved continental back-arc basins ($\sum$HREE = 17–19, Saunders & Tarney 1979). The LREE content ($\sum$LREE = 46–78) is slightly higher than shown by these rocks (E-MORB = 46, back-arc thol = 44). This LREE enrichment is probably caused by crustal contamination processes, evidenced by the cerium anomaly.

The acid metavolcanic tuffs and rhyolitic metaporphyries of aluminous and calcalkaline character

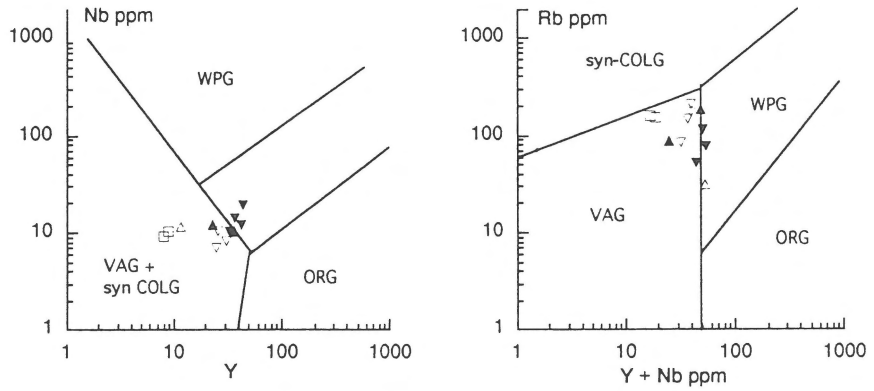

Fig. 11. Nb–Y and Rb–Y+Nb diagrams after Pearce et al. (1984). Acid rocks are distributed among compressive (VAG = volcanic-arc granites) and extensive domains (WPG = intra-plate granites). Symbols as in Fig. 3.

represent essentially crustal melts. However, there are significant geochemical variations among them. The lower metatuffs of the Cadaqués series are geochemically more differentiated than the Upper series metatuffs; likewise, they are intermediate between the upper metatuffs and quartz-monzonitic metaporphyry (Port orthogneiss) located in the lowermost part of the sequence. On the other hand, the rhyolitic metaporphyries display geochemical features suggesting that they are the more impoverished melt.

Logarithmic correlation diagrams for zirconium against major and trace elements (Fig. 9) do not show clear positive trends for FeO_T, TiO_2, CaO, Cr and V between the metatuffs and rhyolitic metaporphyries. Neither is there a correlation between these elements in the orthogneisses. On the other hand, on Nb–Y and Rb–Y+Nb diagrams (Pearce et al. 1984; Fig. 11) the assemblages of acid magmatic rocks plot between the volcanic-arc and intraplate areas. Likewise, SiO_2-Nb ratios (Nb < 12 ppm, Pearce & Gale 1977) are in accordance with a crustal origin related to subduction environments for the metatuffs and the rhyolitic metaporphyries; their plot on the Q-Ab-Or diagram places them in the area of crustal melting.

The incompatible elements and REE spidergrams for the metavolcanic acid rocks (Figs 7a, b, 8a) show patterns similar to those of crustal melts (S-type magmas, Thompsom et al. 1984). However, in the lower metarhyolites an analogy can be made with the Port orthogneiss based on their REE patterns, suggesting a continued fractionation combined with hydrothermal contamination and probably separation of a residual garnet phase.

All rhyolitic metaporphyries, regardless of their position in the sequence, are similar. They can be distinguished from the other acid rocks by their depleted incompatible trace elements and REE patterns ($\sum$REE = 58–65, Figs 7d, 8b). The marked negative slope of their incompatible patterns, with distinctive negative anomalies in phosphorus and titanium, suggests a high degree of partial melting and a highly impoverished crustal source.

Acknowledgements

This study has been supported by the Projects PB88 0240 and PB91 0477 of Dirección General de Investigación Científica y Técnica (DGICYT) and the Acción Integrada de Cooperación Franco-Española no. 18A programs. M.N. wishes to thank G. Guitard of Université Pierre et Marie Curie, Paris VI, for his assistance in performing the geochemical analyses of minerals, and M. Muñoz of Petrology Department of Madrid for her suggestions. We specially express our appreciation to the journal referees, Harry N.A. Priem and R.P. Kuijper whose careful reviews and suggestions resulted in improvements of this paper. Thanks are also due to N.J. Snelling of the Geochronology Laboratory of the Complutense University of Madrid for English revision.

References

Besson, M. & M. Fonteilles 1974 Relations entre les comportements contrastes de l'alumine et du fer dans la différenciation des séries

tholéiitique et calco-alcaline – Bull. Soc. Fr. Minerál. Cristal. 97: 445–449

Bienvenue, P., H. Bouggoult, J.L. Joron, M. Treuil & L. Dmitriev 1990 MORB alteration: Rare earth element non-rare earth hygromagmaphile element fractionation – Chem. Geology 82: 14

Brouxel, M., C. Lecuyer & H. Lapierre 1989 Diversity of magma types in a lower Paleozoic island arc-marginal basin system (Eastern Klamath Mountains, California, USA) – Chem. Geology. 77: 251–264

Cabanis, B. 1986 Identification des séries magmatiques dans les socles métamorphiques sur la base de critères géologiques, pétrographiques et géochimiques – Thèse Doctorat d'Etat. Univ. Pierre et Marie Curie. Paris VI. 682 pp

Carreras, J. & J. Ramirez 1984 The geological significance of the Port de la Selva Gneisses (Eastern Pyrenees, Spain). In: Sassi & Julivert – IGCP Newsletter 6: 27–31

Debon, F. & P. Le Fort 1983 Chemical mineralogical classification of common plutonic rocks and associations – Trans. Roy. Soc. Edinburgh Earth Sci. 73: 135–149

Dupuy, C. & J. Dostal 1984 Trace element geochemistry of some continental tholeiites – Earth. Planet. Sci. Lett. 67: 61–69

Govindaraju, K. & G. Mevelle 1987 Fully automated dissolution and separation methods for inductively coupled plasma atomic emission spectrometry rock analysis. Application to the determination of rare earth elements – J. Anal. Atom. Spectrom 2: 615–621

Guitard, G. 1970 Le métamorphisme hercynien mésozonal et les gneiss oeillés du massif du Canigou (Pyrénées orientales) – Mém. Bur. Rech. Geol. Min. 63, 291 pp

Holm, P.E. 1985 The geochemical fingerprints of different tectonomagmatic environments using hygromagmatophile element abundances of tholeiitic basalts and basaltic andesites – Chem. Geology 51: 303–323

Humphris, S.E., G. Thompsom, J.G. Schilling & R.A. Kingsley 1985 Petrological and Geochemical variations along de Mid-Atlantic Ridge between 46° S and 32° S: Influence of the Tristan da Cunha mantle plume – Geochim. Cosmochim. Acta 49: 145–164

Humphris, S. & R.H. Thompson 1978 Trace element mobility during hydrothermal alteration of oceanic basalts – Geochim. Cosmoch. Acta 42: 127–136

Knoper, M.W. & K.C. Condie 1988 Geochemistry and petrogenesis of early Proterozoic amphibolites west-central Colorado, USA – Chem. Geology 67: 209–225

Kuno, H. 1959 Origin of Cenozoic petrographic provinces of Japan and surrounding areas – Bull. Volc. 20: 37–76

Laumonier, B. 1988 Les Groupes de Canaveilles et de Jujols ("Paléozoïque inférieur") des Pyrénées Orientales, arguments en faveur de l'age essentiellement Cambrien de ces Séries – Hercynica 4: 25–38

Laumonier, B. & G. Guitard 1986 Le Paléozoïque inférieur de la moitié orientale de la zone axiale des Pyrénées. Essai de synthèse – C. R. Acad. Sci. Paris 302 (II): 473–478

Leake, B.E. 1978 Nomenclature of amphiboles – Miner. Magazine 42: 533–563

Miyashiro, A. 1974 A volcanic rock series in island arcs and active continental margins – Amer. J. Sci. 274: 321–355

Mullen, E.D. 1983 $MnO/TiO_2/P_2O_5$: A minor element discriminant for basaltic rocks of oceanic environments and its implications for petrogenesis – Earth Planet. Sci. Lett. 62: 53–62

Pearce, J.A. & J.R. Cann 1973 Tectonic setting of basic volcanic rocks determined using trace elements analysis – Earth Planet. Sci. Lett. 19: 290–300

Pearce, J.A. & G.H. Gale 1977 Identification of ore deposition environment from trace-element geochemistry of associated igneous host rocks. In: Volcanic processes in ore genesis. The Institution of Mining and Metallurgy. London: 14–25

Pearce, J.A., B. Nigel, W. Harris & A.G. Tindle 1984 Trace element discrimination diagrams for the tectonic interpretation of granitic rocks – J. Petrol. 25: 956–983

Pecerrillo, A. & S.R. Taylor 1976 Geochemistry of Eocene calc-alkaline volcanic rocks from the Kastamonu area, Northern Turkey – Contrib. Miner. Petrol. 58: 63–81

Prinzhofer, A. & C.J. Allegre 1985 Residual peridotites and the mechanism of pertial melting – Earth Planet. Sci. Lett. 74: 179–203

Ramirez, J. 1983 Els gneiss de Port de la Selva: Significació petrològica i relacions amb l'encaixant. Tesi de Llicenciatura. Univ. Barcelona, 210 pp

Saunders, A.D. & S. Tarney 1979 The geochemistry of basalts from a back-arc spreading centre in the East Scotia Sea – Geochim. Cosmoch. Acta 43: 555–572

Saunders, A.D., S. Tarney & S.D. Weaver 1980 Transverse variations across the Antartic peninsula: implications for the genesis of calc-alkaline magmas. Earth Planet. Sci. Lett. 46: 344–360

Stolz, A., R. Varne, G.R. Davies, G. Wheller & D. Foden 1990 Magma source components in an arc-continental collision zone: the Flores-Lambata sector, Sunda arc, Indonesia – Contrib. Miner. Petrol. 105: 585–601

Taylor, S.R. & S.H. MacLennan 1985 The continental Crust: its Composition and Evolution. Blackwell Scientific Publ. 311 pp

Thompsom, R.N., M.A. Morrison, G.L. Hendry & S.J. Parry 1984 An assessment of the relative roles of crust and mantle in magma genesis: an elemental approach – Phil. Trans. R. Soc. London 310: 549–590

Winchester, J.A. & P.A. Floyd 1976 Geochemical magma type discrimination: Application to altered and metamorphosed basic igneous rocks – Earth Planet. Sci. Lett. 28: 459–469

Winchester, J.A. & P.A. Floyd 1977 Geochemical distributions of different magma series and their differentiation products using immobile elements – Chem. Geol 20: 325–343